Cr^{3+}/COO^- Complexation Induced Aggregation of Gelatin in Dilute Solution

Wei Lin,[†,‡] Yunshen Zhou,[†] Yuer Zhao,[†] Qingshi Zhu,[†] and Chi Wu*[,†,§]

Laboratory of Bond-Selective Chemistry, Department of Chemical Physics, University of Science and Technology of China, Chinese Academy of Sciences, Hefei, 230026, Anhui, China; Institute of Biomass Engineering, The Key Laboratory of Leather Chemistry and Engineering of Ministry of Education, Sichuan University, Chengdu, 610065, Sichuan, China; and Department of Chemistry, The Chinese University of Hong Kong, Shatin, N.T., Hong Kong

Received March 11, 2002; Revised Manuscript Received May 30, 2003

ABSTRACT: The Cr^{3+}/COO^- complexation induced aggregation of linear gelatin chains in aqueous solutions under different conditions, such as the Cr^{3+} and gelatin concentrations, was investigated by a combination of static and dynamic laser light scattering (LLS). The results reveal a competition between the intrachain and interchain complexation. For a given gelatin concentration, there exists a "critical" Cr^{3+} concentration at which the interchain complexation became dominant. The intensity $I(q)$ of the light scattered from the resultant aggregates was scaled to the scattering vector q as $I(q) \propto q^{-d_q}$ with d_q = 1.61−1.84, suggesting that the aggregation was a diffusion-limited process. The variation of the Cr^{3+} concentration had less influence on the structure of the resultant aggregates. On the other hand, the decrease of the gelatin concentration led to an increase of d_q from 1.61 to 2.04, indicating that the aggregation changed from a diffusion-limited process to a reaction-limited one. Precipitation is independent of the size of the aggregates but closely related to the gelatin concentration as well as the Cr^{3+}/gelatin molar ratio. Two-dimensional AFM topographs of the aggregates revealed a clear growing fractal, supporting the results observed by LLS.

Introduction

The metal ion induced aggregation of polyampholytes chains in solution is both a fascinating academic research topic and important in industry.[1] It affects protein denaturation, enzymatic reaction, coagulation, purification, and concentration. Gelatin is a denatured protein and biodegradable, normally obtained from the breakdown of the ordered helical collagen.[2] As other proteins, gelatin is an amphoteric polyelectrolyte with both positively and negatively charged amino acids interspersed on the chain backbone. It is well-known that Cr^{3+} can strongly interact with the side carboxyl group of aspartic and glumatic acids of collagen via the metal-ion-mediated two-point or multipoint coordination.[3,4] Therefore, Cr^{3+} as a good protein stabilizer has been utilized in the tanning industry for more than a century.[5] Moreover, Cr^{3+} as a cross-linking agent has recently been used in the immobilization of enzymes[6−8] and the controlled release of drugs.[9]

In the past, numerous theoretical and experimental efforts have been devoted to the formation and structure of colloidal aggregates.[10−13] Mandelbrot[14] used the name *fractal* to describe a rather special kind of complexes. As research developed in this direction, it was found that the fractal growth was closely related to the aggregation of similar particles,[15] resulting in the objects with complicated geometries. Two limiting regimes have been identified as the diffusion-limited cluster−cluster aggregation (DLCA) and the reaction-limited cluster−cluster aggregation (RLCA).[16−18] One of the distinctive features between DLCA and RLCA is that the resultant aggregates have different fractal dimensions (d_f), i.e., different scalings between the mass (M) and size (R) of the aggregates, $M \sim R^{d_f}$. In DLCA, two particles irreversibly stick together as soon as they collide with each other. The aggregation rate is solely determined by the time required for two particles diffuse to each other.[15] The approaching particle has less chance to penetrate into a cluster, resulting in a loose and open structure with d_f in the range 1.75−1.80 for a three-dimensional system.[19,20] The kinetics of DLCA is characterized by a power law $R \sim t^{\alpha}$ with $\alpha < 1$, where t is the aggregation time.[21] On the other hand, the sticking probability (or collision efficiency) in RLCA is so low that many collisions could only lead to one sticking. Therefore, the approaching particle has a much better chance to interpenetrate into a cluster to form more uniform structures with a higher fractal dimension d_f in the range 2.0−2.5, depending on experimental conditions.[15,22,23] The RLCA process follows exponential kinetics, $R \sim e^{At}$, where A is a system-dependent constant.[21]

Laser light scattering (LLS) is a particular useful method to study the aggregation process because it can continuously monitor the aggregation in a noninvasive manner, especially in dilute solution.[24−27] In the study of the formation and structure of aggregates, a combination of static and dynamic LLS can provide not only the size of the aggregates but also the mass (aggregation number) and density distribution of the aggregates for a wide variety of colloidal systems. Divalent cation (Ca^{2+}) induced aggregation of synthetic polyelectrolytes and gelatin have recently been studied.[23,28] To our knowledge, the LLS study of trivalent chromium cation induced self-aggregation of gelatin has been limited so far. In addition, atomic force microscopy (AFM) has recently been developed as a routine technique to image nonconductive biological macromolecules with a high

† Chinese Academy of Sciences.
‡ Sichuan University.
§ The Chinese University of Hong Kong.
* The Hong Kong address should be used for correspondence. E-mail: chiwu@cuhk.edu.hk.

10.1021/ma020372n CCC: $22.00
Published on Web 08/13/2002

resolution,[29] such as the structure of individual biopolymers and supramolecular assemblies.[30−32] It is our intention in this study to use LLS combined with AFM to investigate the effect of the Cr^{3+} and gelatin concentrations on the cation/COO^- complexation induced aggregation in buffer solution. The AFM topographic images of two-dimensional gelatin aggregates will give us direct evidence of the fractal structure of the resulting aggregates.

Experimental Section

Solutions Preparation. The gelatin (courtesy of BASF, Germany) is alkali pretreated with an isoelectric point (IEP) of pH = 4.9−5.1.[19] To obtain a complete dissolution in water, the stock solution was prepared as follows. First, the gelatin was dissolved in a small amount of formamide at 45 °C for 2 h. The formamide solution was kept at 20 °C for 24 h before it was transferred into deionized water (≥18.2 MΩ, Milli-Q, Millpore). The formamide/water weight ratio was kept at 2%. 1 mM sodium azide (NaN_3) was added to prevent bacterial growth. The final concentration of such prepared gelatin stock solution was 1.0×10^{-3} g/mL, which was diluted to different desired concentrations. For the Cr^{3+}/COO^- complexation induced aggregation, the pH of the gelatin solutions used was adjusted to 7.5 with a Tris buffer. The complexation was induced by adding a proper amount of dust-free basic chromium sulfate (Bayer, Germany) aqueous solution dropwise into 2 mL of dust-free gelatin solution. Three gelatin concentrations (1.0×10^{-4}, 3.0×10^{-4}, and 5.0×10^{-4} g/mL) were used. The gelatin and chromium solutions were respectively clarified with a 0.45 μm Millipore millex filter and a 0.1 μm Whatman anotop filter to remove dust.

Laser Light Scattering. A modified commercial LLS spectrometer (ALV/SP-125, Germany) was used, which equipped a solid-state laser (Coherent DPSS) with an output power of 400 mW at $\lambda_0 = 532.0$ nm and an ALV-5000 multi-τ digital time correlator. All the LLS measurements were performed at 25 °C. The details of the LLS instrument action and theory can be found elsewhere.[33] For the convenience of discussion, only the basic principle is outlined as follows. In static LLS, the angular dependence of the absolute excess time-average scattered intensity, known as the Rayleigh ratio $R_{vv}(q)$, is measured, where q is the scattering vector. For a very dilute solution at scattering angle θ, $R_{vv}(q)$ can be related to the weight-average molar mass M_w, the z-average root-mean-square radius of gyration $\langle R_g^2\rangle_z^{1/2}$ (or written as $\langle R_g\rangle$) of the scattering objects, and the second virial coefficient A_2 by[34]

$$\frac{KC}{R_{vv}(q)} \approx \frac{1}{M_w}\left(1 + \frac{1}{3}\langle R_g^2\rangle_z q^2\right) + 2A_2C \text{ (Zimm plot)} \quad \text{for } \langle R_g^2\rangle^{1/2} q < 1$$

$$\frac{KC}{R_{vv}(q)} \approx \frac{1}{M_w \exp\left(-\frac{1}{3}R_g^2 q^2\right)} + 2A_2C \text{ (Guinier plot)} \quad \text{for } \langle R_g^2\rangle^{1/2} q > 1 \quad (1)$$

where C is the polymer concentration in the unit of g/mL, $K = 4\pi^2 n^2 (dn/dc)^2/(N_A\lambda_0^4)$, and $q = (4\pi n/\lambda_0)\sin(\theta/2)$, with n, dn/dc, N_A, and λ_0 being the refractive index of solvent, the specific refractive index increment, the Avogadro constant, and the wavelength of laser light in a vacuum, respectively. For an aggregate with a fractal geometry and made of colloid particles, the scattered intensity $I(q)$ is scaled to q as $I(q) \sim q^{-d_f}$ in the range of $R_{aggregate} > q^{-1} > R_0$, where d_f is the fractal dimension and $R_{aggregate}$ and R_0 are the radii of the aggregate and primary particle, respectically.[15,17,27]

In dynamic LLS, the Laplace inversion or cumulant analysis of the measured intensity−intensity time correlation function $G^{(2)}(t,q)$ can result in a line-width diffusion coefficient distribution $G(\Gamma)$ or an average line-width $\langle\Gamma\rangle$. For a diffusive relaxation, Γ is related to the diffusion coefficient D by $D = (\Gamma/q^2)_{q\to 0, C\to 0}$ or the hydrodynamic radius R_h by the Stokes−Einstein equation, $R_h = k_BT/(6\pi\eta D)$, with k_B, T, and η the Boltzmann constant, the absolute temperature, and the solution viscosity, respectively. Therefore, $G(\Gamma)$ can be converted to a hydrodynamic radius distribution $f(R_h)$. The CONTIN Laplace inversion program in the correlator was used. All the static and dynamic LLS measurement were done at 25 °C.

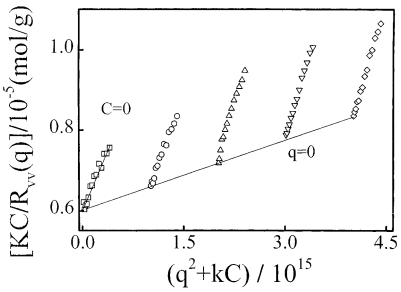

Figure 1. Typical Zimm plot of gelatin in aqueous solution at T = 25 °C, pH = 6.4, where the solution contained 2% formamide, K is a constant, the gelatin concentration ranged from 1.0×10^{-4} to 5.0×10^{-4} g/mL, and k is a spreading constant.

Table 1. Laser Light Scattering Results of Gelatin and Its Aggregates in Aqueous Solution at 25 °C

$[Cr^{3+}]/\mu$M	$[Cr^{3+}]$/gelatin	M_w/(g/mol)	$\langle R_h\rangle$/nm	$\langle R_g\rangle$/nm
0	0	1.6×10^5 [a]	22.3	38
0	0	4.8×10^5	40.1	60
3.1	2.95	5.9×10^5	44.8	67
6.2	5.92	7.0×10^5	56.2	70
9.2	8.83	8.5×10^5	79.0	78
15.5	14.9	1.4×10^6	108	98
22.9	22.2	1.9×10^6	118	106
30.3	29.4	2.8×10^6	146	127
37.6	36.9	4.2×10^6	169	143
57.6	55.4	8.1×10^6	212	177
85.9	83.4	1.6×10^7	254	196
114	110	2.5×10^7	302	224
142	139	3.8×10^7	362	258
167	167	5.1×10^7	377	273
196	194	4.6×10^7	367	267
223	223	3.7×10^7	365	263

[a] It was determined at pH = 6.4, and the rest results were obtained at pH = 7.5.

Atomic Force Microscopy. A commercial AFM (Nanoscope IIIa, Digital Instrument Inc., Santa Barbara, CA) equipped with a 180 μm scanner (j-scanner) and a Tapping Mode etched silicon probe (TESP) was used. The cantilever (160 μm in length) and the probe were an integrated assembly of single-crystal silicon. All the topographic images were recorded in the tapping mode at a constant force. The same solution was used for both LLS and AFM. A piece of freshly cleaved mica (ca. 1.0 cm × 1.0 cm) was dipped into the solution for ~2 s and then dried before it was imaged by AFM. To minimize possible contamination of the surface by ambient air, each sample was freshly prepared just before the AFM study.

Results and Discussion

Figure 1 shows a typical Zimm plot of gelatin in aqueous solution at pH = 6.4 and 25 °C, where C ranged from 2.5×10^{-4} to 1.0×10^{-3} g/mL, which incorporates the angular and concentration extrapolations of $R_{vv}(q)$ on a single grid. On the basis of eq 1, the extrapolation of $[KC/R_{vv}(q)]_{q\to 0, C\to 0}$ leads to M_w. The slopes of $[KC/R_{vv}(q)]_{C\to 0}$ vs q^2 and $[KC/R_{vv}(q)]_{q\to 0}$ vs C respectively lead to $\langle R_g\rangle$ and A_2. The values of $M_{w,chain}$, $\langle R_g\rangle$, and $\langle R_h\rangle$ determined from LLS are summarized in Table 1. The slightly positive value of A_2 (1.16×10^{-3} mol mL/g^2) indicates that the mixed solvent at pH = 6.4 was a marginally good (close to the Θ point) solvent for gelatin.

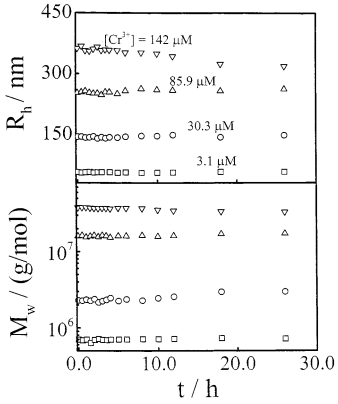

Figure 2. Time dependence of average hydrodynamic radius $\langle R_h \rangle$ and weight-average molar mass M_w of gelatin aggregates formed in the presence of different amounts of Cr^{3+}, where the gelatin concentration was 1.0 μM, pH = 7.5, and T = 25 °C.

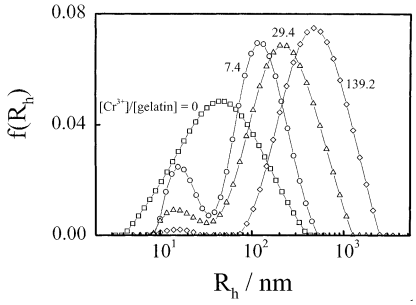

Figure 3. $[Cr^{3+}]$/[gelatin] molar ratio dependence of the hydrodynamic radius distribution $f(R_h)$ of gelatin aggregates, where the gelatin concentration was 1.0 μM, pH = 7.5, and T = 25 °C.

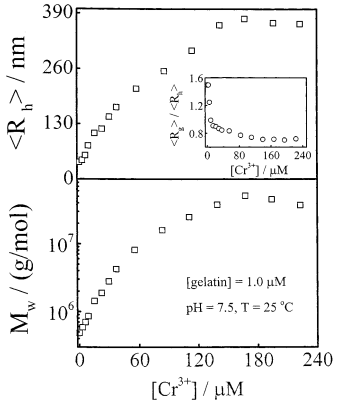

Figure 4. Cr^{3+} concentration dependence of average hydrodynamic radius $\langle R_h \rangle$ and weight-average molar mass M_w. The inset shows a corresponding Cr^{3+} concentration dependence of ratio of average radius of gyration to average hydrodynamic radius $\langle R_g \rangle / \langle R_h \rangle$.

It is known that for monodispersed liner flexible polymer chains in a good solvent,[36] $\langle R_g \rangle / \langle R_h \rangle \sim 1.5$. Here $\langle R_g \rangle / \langle R_h \rangle$ (~1.8) is slightly higher, reflecting that the gelatin chains used were polydispersed.

Figure 2 shows the Cr^{3+} concentration dependence of the Ca^{2+}/COO^- complexation induced aggregation, where the gelatin concentration was kept at 1.0 μM (=4.8 × 10^{-4} g/mL). Note that the complexation was so fast that our present LLS setup was not able to detect the initial change of either M_w or $\langle R_h \rangle$. Here, we started the measurement ~5 min after adding Cr^{3+}. It has been found that when $[Cr^{3+}] \leqslant \sim 3$ μM, i.e., on average three

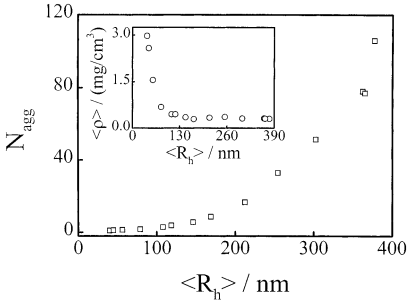

Figure 5. Size dependence of average number of chains inside each aggregation(N_{agg}), where $N_{agg} = M_{w,aggregate}/M_{w,chain}$. The inset shows average chain density $\langle \rho \rangle$ of gelatin aggregates, where $\langle \rho \rangle = M_{w,aggregate}/(4/3)\pi(R_h)^3 N_A$ and N_A is the Avogadro constant; the gelatin concentration was 1.0 μM, pH = 7.5, and T = 25 °C.

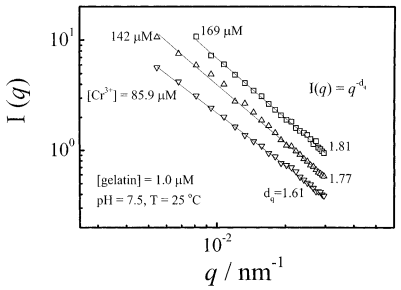

Figure 6. Double-logarithmic plot of scattering intensity $I(q)$ vs scattering vector q for gelatin aggregates formed at different Cr^{3+} concentration, where d_f is the fractal dimension of resultant aggregates.

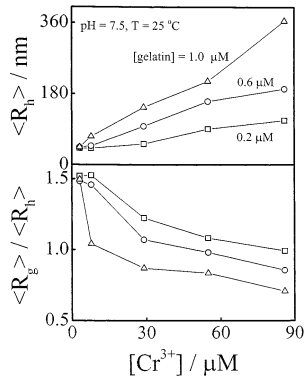

Figure 7. $[Cr^{3+}]$ concentration dependence of average hydrodynamic radius $\langle R_h \rangle$ and ratio of average radius of gyration to average hydrodynamic radius ($\langle R_g \rangle / \langle R_h \rangle$) of gelatin aggregates formed at different gelatin concentrations.

Cr^{3+} ions per gelatin chain, there was essentially no change in both M_w and $\langle R_h \rangle$, indicating that there existed little interchain complexation. Presumably, most of Cr^{3+} were coordinated within individual gelatin chains. Note that in the low and medium $[Cr^{3+}]$ the resultant solutions were stable without any observable precipitation up to ~6 days. At higher $[Cr^{3+}]$, the aggregates became unstable and tended to coagulate to form cottonlike precipitation after 4−6 h, reflecting in the decrease of both M_w and $\langle R_h \rangle$ in Figure 2. The Cr^{3+} concentration range in which the solution changed from stable to coagulating was rather narrow. A further increase of Cr^{3+} immediately led to precipitation. Figure 3 clearly reveals the competition between the intrachain and interchain aggregation. As $[Cr^{3+}]$ increases, the hydrodynamic radius distributions $f(R_h)$ splits from one peak into two peaks, indicating the interchain dominant complexation at higher $[Cr^{3+}]$/[gelatin] ratios.

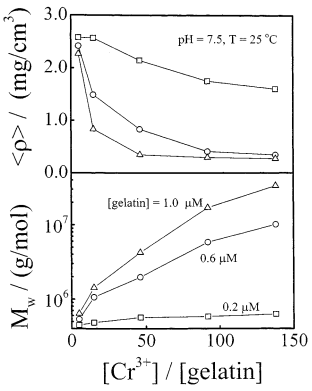

Figure 8. $[Cr^{3+}]$/[gelatin] molar ratio dependence of average chain density $\langle\rho\rangle$ and weight-average molar mass M_w of gelatin aggregates formed at different initial concentrations, where $\langle\rho\rangle = M_{w,aggregate}/(4/3)\pi(R_h)^3N_A$ with N_A the Avogadro constant.

Figure 4 shows the Cr^{3+} concentration dependence of $\langle R_h\rangle$ and M_w of the gelatin aggregates, where both M_w and $\langle R_h\rangle$ were obtained from stable aggregates. There existed a "critical" concentration $[Cr^{3+}]_{agg}$ for the interchain Cr^{3+}/COO^- complexation. When $[Cr^{3+}] > [Cr^{3+}]_{agg}$, both M_w and $\langle R_h\rangle$ significantly increased, revealing a clear interchain aggregation. Over a wide range of $[Cr^{3+}]$, both M_w and $\langle R_h\rangle$ increased with $[Cr^{3+}]$, reflecting that Cr^{3+} acted as a cross-linking agent to connect the gelatin chains together by two-point or multipoint Ca^{2+}/COO^- complexation. When $[Cr^{3+}]/[\text{gelatin}] \geqslant \sim 170$, the precipitation started, reflected in the decrease of M_w. The values of M_w, $\langle R_g\rangle$, and $\langle R_h\rangle$ formed at different Cr^{3+}/gelatin molar ratios are summarized in Table 1.

Figure 5 shows an expected increase of the average number of the gelatin chains per aggregate (N_{agg}) as the size of the aggregate increases. The decrease of the average chain density $\langle\rho\rangle$ in the inset clearly indicates that the aggregates become loose and less uniform, presumably with a fractal structure. Such a fractal structure is clearly reflected in the scaling between the scattered light intensity $I(q)$ and scattering vector q, as shown in Figure 6, i.e., $I(q) \sim q^{-d_q}$, where d_q is in the range 1.6−1.8, suggesting that the Cr^{3+}/COO^- complexation induced gelatin aggregation was a diffusion-limited process, and the resultant aggregates had an open and loose structure. The similar scaling between $I(q)$ and q for the aggregates with different sizes shows that the structure of the aggregates is nearly independent of $[Cr^{3+}]$ as long as the aggregate reaches a certain size.

To study the effect of the gelatin concentration on the aggregation, two more gelatin solutions (0.2 and 0.6 μM) were also examined. Figures 7 and 8 compare the $[Cr^{3+}]$/[gelatin] dependence of the aggregation of three gelatin solutions in terms of $\langle R_h\rangle$, $\langle R_g\rangle/\langle R_h\rangle$, M_w, and $\langle\rho\rangle$. It was found that for a given $[Cr^{3+}]$ the solution with a lower gelatin concentration tended to precipitate because the ratio of $[Cr^{3+}]/[COO^-]$ was higher. A comparison of Figures 2, 7, and 8 shows that the precipitation was not directly related to the size of the aggregates. In fact, when the gelatin concentration was lower, the resultant aggregates were smaller when the precipitation occurred.

Figure 7 shows that the size of the aggregates increases with the Cr^{3+} concentration. In Figure 5, we already saw that the chain density of the aggregate decreased as $\langle R_h\rangle$ increased, which is also reflected in Figure 8. Figure 8 further shows that for a given $[Cr^{3+}]$/[gelatin] the larger aggregates formed at higher gelatin concentrations have a lower chain density $\langle\rho\rangle$, indicating that they have a looser structure. When $[Cr^{3+}]$/[gelatin] reached ~140, the most dilute gelatin solution (0.2 μM) was stable, but the other two gelatin solutions (0.4 and 1.0 μM) started to precipitate a few hours after the addition of Cr^{3+}. This showed that both the gelatin concentration and the Cr^{3+}/gelatin molar ratio were related to the precipitation.

As discussed before, intrachain Cr^{3+}/COO^- complexation results in the contraction of individual gelatin chains. Only intermolecular Cr^{3+}/COO^- complexation can lead to the aggregation. Such two processes always compete with each other. In a relatively concentrated gelatin solution, the interchain complexation is so dominant that larger clusters are formed, while in a more diluter gelatin solution, individual chains have a better chance to undergo intrachain contraction before the interchain aggregation via the COO^- groups remaining on the periphery of collapsed gelatin chains. On the other hand, the intrachain Cr^{3+}/COO^- complexation is less effective than the interchain complexation because of the chain rigidity. Therefore, the aggregates formed in a relatively dilute solution are much smaller. Such aggregates involve less chain interpenetrating so that their chain density is higher, as shown in Figure

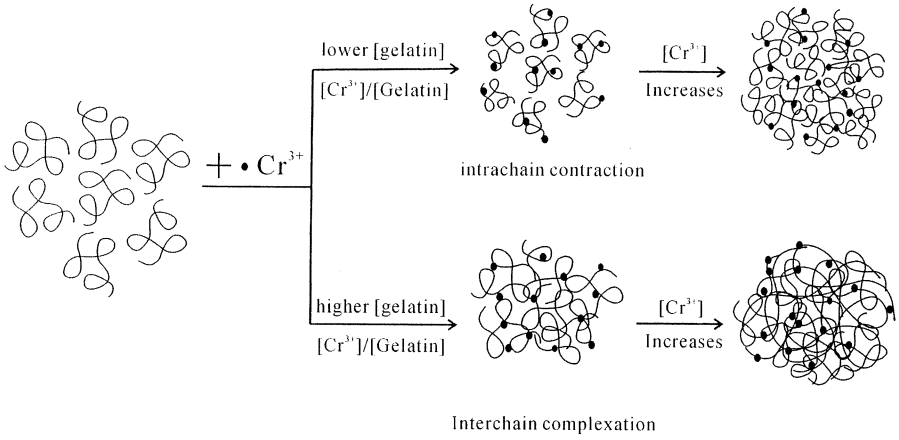

Figure 9. Schematic of Cr^{3+}/COO^- complexation induced aggregation of linear gelatin chains under different experimental conditions. At lower gelatin concentrations or Cr^{3+}/gelatin molar ratio, the linear gelatin chain first undergoes intrachain contraction before interchain aggregation. While at higher gelatin concentrations or higher Cr^{3+}/gelatin molar ratio, intrachain contraction and interchain aggregation happen simultaneously.

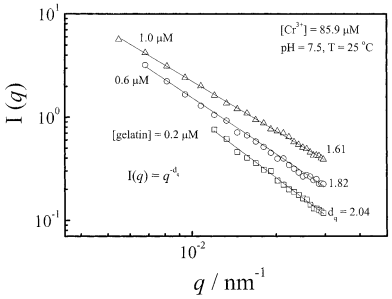

Figure 10. Double-logarithmic plot of scattering intensity $I(q)$ vs scattering vector q for the gelatin aggregates formed at different gelatin concentrations and a given Cr^{3+} concentration.

8. In addition, the chain contraction induced by the intrachain complexation can force the hydrophilic groups such as $-COOH$, $-OH$, and $-NH_3^+$ to its periphery, stabilizing the aggregates. Therefore, the precipitation is apparently related to the Cr^{3+}/COO^- molar ratio and gelatin concentration, reflecting the competition between the intrachain and interchain complexation. Figure 9 shows a schematic of such an intrachain and interchain complexation.

Figure 10 shows that for a given $[Cr^{3+}]$ the fractal dimension increases as the gelatin concentration decreases. This can also be attributed to the intrachain and interchain complexation. In a more diluted gelatin solution, the aggregates are formed from individual contracted gelatin chains. The sticking probability between the contracted chains are relatively small since the collapsed chains are more mobile in solution, so that only a number of collisions result in sticking. Thus, two collided clusters have more time to penetrate each other. This is why the aggregates formed in a dilute solution have a more uniform chain density and a higher fractal dimension, as shown schematically in Figure 9.

Figure 11 shows the AFM topographs of the aggregates formed in the presence of different amounts of Cr^{3+}. For a given gelatin concentration, the number of the aggregates decreased as the Cr^{3+} concentration increased, but the aggregates became larger and irregular. Note that here the three-dimensional clusters

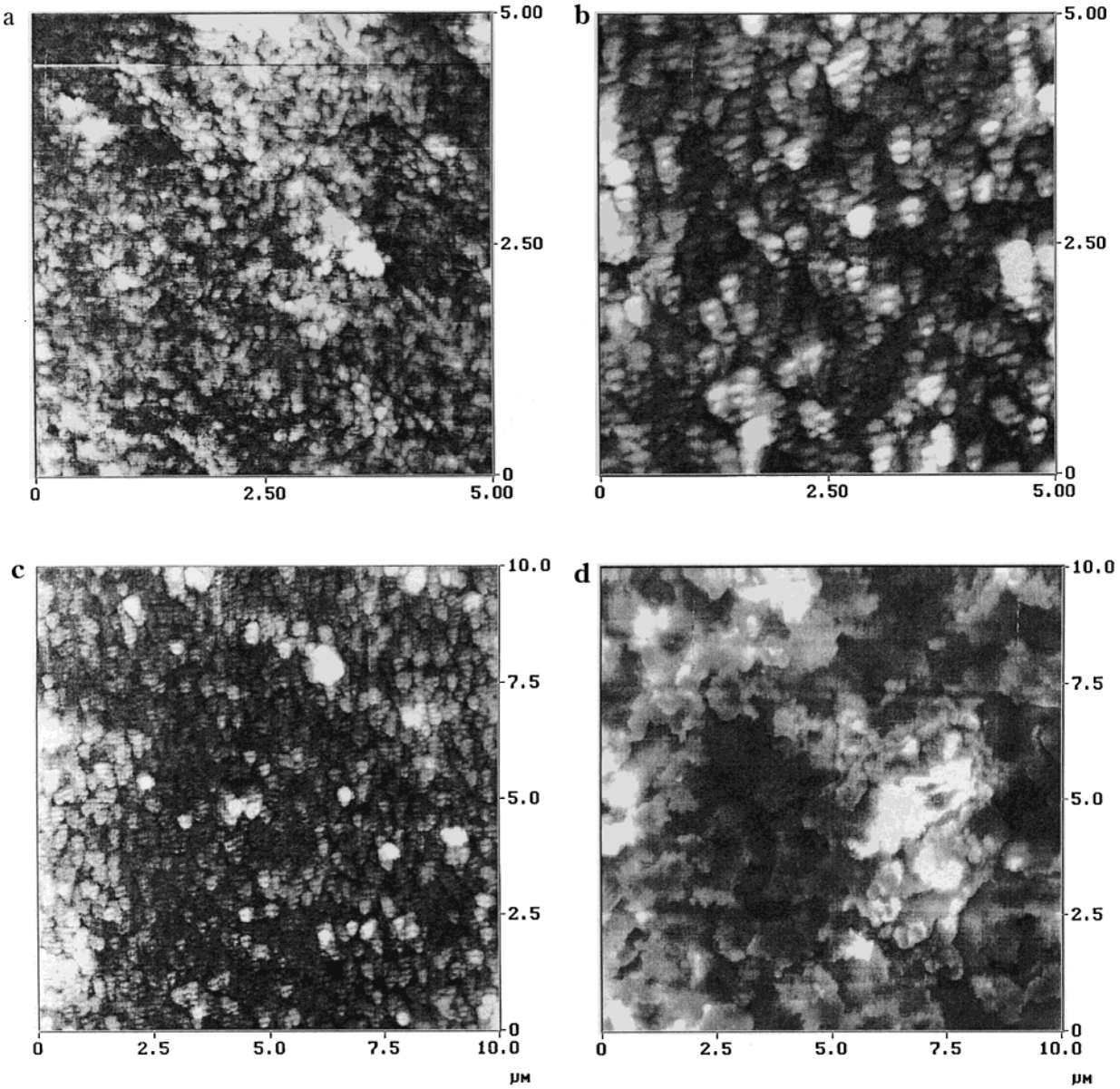

Figure 11. Tapping-mode AFM images of gelatin aggregates at $T = 25$ °C and [gelatin] = 1.0 μM: (a) $[Cr^{3+}] = 3.1$ μM; (b, c) $[Cr^{3+}] = 85.9$ μM; (d) $[Cr^{3+}] = 142$ μM.

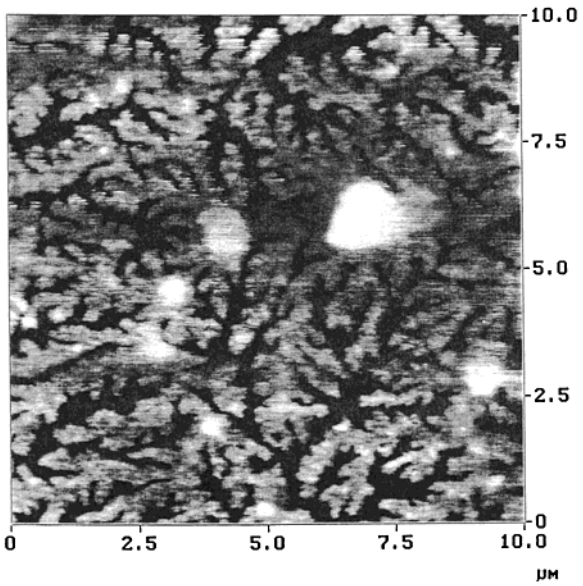

Figure 12. Tapping-mode AFM images of gelatin aggregates formed at [gelatin] = 0.2 μM, [Cr^{3+}] = 85.9 μM, and T = 25 °C.

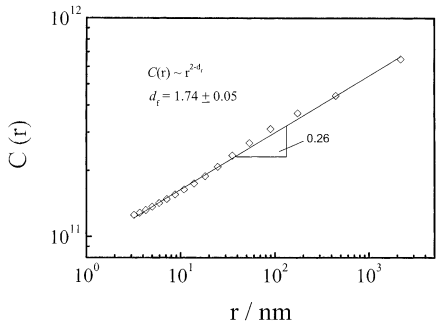

Figure 13. Double-logarithmic plot of density correlation function $C(r)$ vs distance r of the gelatin aggregates at two-dimensional substrate, where [gelatin] = 0.2 μM and [Cr^{3+}] = 85.9 μM.

were projected onto a two-dimensional substrate. Parts b and c of Figure 11 were from the same sample but with different amplification. Nonetheless, the loose and ramified characteristics on the periphery of the aggregates are well reflected in Figure 11d. Figure 12 shows that, in a more dilute gelatin solution, the aggregates clearly have a fractal geometry. The fractal dimension (d_f) of the aggregates can be determined from the density correlation function $C(r) \sim r^{2-d_f}$,[15] as shown in Figure 13. Note that the value of d_f obtained from the AFM topograph is close to the values (~1.7) in the literature for the two-dimensional reaction-limited cluster−cluster aggregation,[10,15,39] supporting the LLS results.

Conclusions

A combination of laser light scattering (LLS) and atomic force microscopy (AFM) studies of the Cr^{3+}/COO^- complexation induced aggregation of linear gelatin chains in aqueous solution at T = 25 °C and pH = 7.5 has revealed a clear competition between the intrachain and interchain complexation. The intrachain complexation resulted in the chain contraction, while the interchain complexation contributed to the aggregation. For a given gelatin concentration, the interchain complexation became dominant when the Cr^{3+} concentration reached a "critical" value. The aggregates formed in a relatively concentrated gelatin solution had a loose and open structure with a fractal dimension (d_q) in the range 1.61−1.84. The increase of [Cr^{3+}] led to larger aggregates, but it had less effect on the diffusion-limited cluster−cluster aggregation (DLCA) mechanism. On the other hand, the gelatin concentration had much more influence on the aggregation. For a given Cr^{3+} concentration, the decrease of the gelatin concentration resulted in aggregates with a higher fractal dimension. At the same time, the aggregation changed from a diffusion-limited to a reaction-limited process. The precipitation induced by the complexation was less dependent on the size of the aggregates but more related to their structures. The two-dimensional AFM topographs of the aggregates also showed that, for a given gelatin concentration, the increase of [Cr^{3+}] could result in looser, but large and irregular, aggregates. In a more dilute gelatin solution, we could directly observe the fractal structure of the resultant aggregates.

Acknowledgment. Financial support of the National Project for the Development of Key Fundamental Sciences in China (G1999075305), CAS Bai Ren Project, the NNSFC projector (29974027), and Kuancheng Wang Postdoctoral Work Fund is gratefully acknowledged. The authors also thank Professor Ziqing Wu, Dr. Bin Wang, and Dr. Bing Li for the process of the AFM images.

References and Notes

(1) Kudaibergenov, S. E. *Adv. Polym. Sci.* **1999**, *144*, 115.
(2) Veis, A. *The Macromolecular Chemistry of Gelatin*; Academic Press: London, 1964.
(3) Gustavson, K. H. *J. Am. Chem. Soc.* **1952**, *74*, 4608.
(4) Heidemann, E. *Fundermentals of Leather Manufacturing;* Eduard Rorther KG Druckerei und Verlag: Darmstadt, 1993.
(5) Knapp, F. *J. Am. Leather Chem. Assoc.* **1921**, *16*, 658.
(6) Elcin, Y. M.; Akbulut, U. *Biomaterials* **1992**, *13*, 156.
(7) Sungur, S.; Akbulut, U. *J. Chem. Technol. Biotechnol.* **1994**, *59*, 303.
(8) Yildirim, O.; Akbulut, U.; Arinc, E.; Sungur, S. *Biomaterials* **1994**, *15*, 587.
(9) Sungur, S.; Emregul, E. *J. Macromol. Sci., Pure Appl. Chem.* **1996**, *A33*, 319.
(10) Meakin, P. *Phys. Rev. Lett.* **1983**, *51*, 1119.
(11) Reinecke, H.; Fazel, N.; Dosiere, M.; Guenet, J. M. *Macromolecules* **1997**, *30*, 8360.
(12) Lin, M. Y.; Lindsay, H. M.; Weitz, D. A.; Ball, R. C.; Klein, R.; Meakin, P. *Nature (London)* **1989**, *339*, 360.
(13) Schaefer, D. W.; Martin, J. E.; Wiltzius, P.; Cannell, D. S. *Phys. Rev. Lett.* **1984**, *52*, 2371.
(14) Mandelbrot, B. B. *The Fractal Geometry of Nature;* Freeman: San Franciso, CA, 1982.
(15) Viczek, T. *Fractal Growth Phenomena;* World Scientific: Singapore, 1989.
(16) Zhou, Z.; Chu, B. *J. Colloid Interface Sci.* **1991**, *143*, 356.
(17) Peng, S.; Wu, C. *Macromolecules* **2001**, *34*, 6795.
(18) Burns, J. L.; Yan, Y.; Jameson, G. J.; Biggs, S. *Langmuir* **1997**, *13*, 6413.
(19) Meakin, P.; Wasserman, Z. R. *Phys. Lett.* **1984**, *103A*, 337.
(20) Jullien, R. *Phys. Rev. Lett.* **1985**, *55*, 1697.
(21) Weitz, D. A.; Huang, J. S.; Lin, M. Y.; Sung, J. *Phys. Rev. Lett.* **1985**, *54*, 1416.
(22) Brown, W. D.; Ball, R. C. *J. Phys. A* **1985**, *18*, L517.
(23) Peng, S.; Wu, C. *Macromolecules* **1999**, *32*, 585.
(24) Lin, M. Y.; Lindsay, H. M.; Weitz, D. A.; Ball, R. C.; Klein, R.; Meakin, P. *Phys. Rev. A* **1990**, *41*, 2005.
(25) Aymard, P.; Nicolai, T.; Durand, D.; Clark, A. *Macromolecules* **1999**, *32*, 2542.
(26) Takata, S.; Norisuye, T.; Tanaka, N.; Shibayama, M. *Macromolecules* **2000**, *33*, 5470.
(27) Kim, A. Y.; Berg, J. C. *Langmuir* **2000**, *16*, 2101.
(28) Peng, S.; Wu, C. *Polymer* **2000**, *42*, 7343.

(29) Binning, G.; Quate, C. F.; Gerber, Ch. *Phys. Rev. Lett.* **1986**, *56*, 930.
(30) Theresa, M. M.; David, A. B. *Biopolymers* **1997**, *42*, 133.
(31) Morris, V. J. *Prog. Biophys. Mol. Biol.* **1994**, *61*, 131.
(32) Mcintire, T. M.; Penner, R. M.; Brant, D. A. *Macromolecules* **1995**, *28*, 6375.
(33) Wu, C.; Zhou, S. *Macromolecules* **1995**, *28*, 8381; **1996**, *29*, 1574.
(34) Chu, B. *Laser Light Scattering*, 2nd ed.; Academic Press: New York, 1976; pp 10−90.
(35) Brown, W. *Dynamic Light Scattering*; Oxford Press: New York, 1993.
(36) Wu, C. *J. Polym. Sci., Polym. Phys.* **1994**, *32*, 803.
(37) Winter, H. H. In *Encyclopedia of Polymer Science and Engineering*; John Wiley & Sons: New York, 1989.
(38) Winter, H. H.; Chambon, F. J. *J. Rheol.* **1986**, *30*, 367.
(39) Hurd, A. J.; Schaefer, D. W. *Phys. Rev. Lett.* **1985**, *54*, 1043.

MA020372N